Exciton analysis of many-body wave functions: Bridging the gap between the quasiparticle and molecular orbital pictures

Stefanie A. Bäppler, Felix Plasser,* Michael Wormit, and Andreas Dreuw
Interdisciplinary Center for Scientific Computing, Ruprecht-Karls-University, Im Neuenheimer Feld 368, 69120 Heidelberg, Germany
(Received 5 October 2014; published 26 November 2014)

Exciton sizes and *electron-hole* binding energies, which are central properties of excited states in extended systems and crucial to the design of modern electronic devices, are readily defined within a quasiparticle framework but are quite challenging to understand in the molecular-orbital picture. The intent of this work is to bridge this gap by providing a general way of extracting the exciton wave function out of a many-body wave function obtained by a quantum chemical excited-state computation. This methodology, which is based on the one-particle transition density matrix, is implemented within the *ab initio* algebraic diagrammatic construction scheme for the polarization propagator and specifically the evaluation of exciton sizes, i.e., dynamic charge separation distances, is considered. A number of examples are presented. For stacked dimers it is shown that the exciton size for charge separated states corresponds to the intermolecular separation, while it only depends on the monomer size for locally excited states or Frenkel excitons. In the case of conjugated organic polymers, the tool is applied to analyze exciton structure and dynamic charge separation. Furthermore, it is discussed how the methodology may be used for the construction of a charge-transfer diagnostic for time-dependent density-functional theory.

DOI: 10.1103/PhysRevA.90.052521 PACS number(s): 31.15.ae, 34.70.+e, 82.35.Cd, 82.50.Hp

I. INTRODUCTION

Quantum chemical computations have improved our understanding of organic electronic devices considerably by giving a first-principles description of electronically excited states [1–6]. These methods provide accurate estimates of excitation energies and molecular properties and give detailed insight into the state character through the molecular orbitals (MOs) involved. However, there are a number of properties relevant to organic electronics [7–9], which are usually not considered in this type of approach. These include *electron-hole* binding energies, exciton sizes, and other properties of the exciton within the quasiparticle picture [10]. While these quantities emerge naturally in a solid-state physics context, e.g., when evaluating the Wannier model or the Bethe-Salpeter equation [11–16], they are notoriously difficult to understand in the MO picture. Indeed, a number of researchers have proceeded to include such ideas in a quantum chemical context by computing exciton sizes [17–20] and binding energies [21,22], and by analyzing the correlated *electron-hole* wave function [23–26]. However, here we attempt to provide a general theory bridging the gap between the quasiparticle and MO viewpoints of electronic excitations. Such a theory should (i) be well-defined independent of the wave-function model and give a result for the exact solution, (ii) apply to a wide range of wave-function properties, (iii) be invariant to redundant orbital rotations, and (iv) neither depend on atom-centered basis function nor require a partitioning of the wave function into atom or fragment centered contributions [27].

The purpose of this work is to present such a theory and exemplify its usefulness in the case of the exciton size (i.e., the mean dynamic charge separation or *electron-hole* separation), which is a highly important and often discussed property of excitons [8,11,28–30]. Although it is difficult to comprehend in standard quantum chemistry terms, it can be readily evaluated with the methods presented here.

Quantification of exciton sizes is not only relevant from a fundamental physics perspective but there is also an important methodological component to this issue. It is well known in molecular quantum chemistry that charge-transfer (CT) character undermines the description of excited states with time-dependent density-functional theory (TDDFT) [31,32]. In solid-state physics the same problem appears in a different way: the inability of standard TDDFT to describe excitonic effects and the ensuing bound *electron-hole* pair [15,22,33]. For large molecular systems one may expect that this latter issue comes into play and there is indeed increasing evidence [33–39] that the resulting dynamic *electron-hole* separation has a similarly detrimental effect on TDDFT as directed charge transfer does. In spite of the fact that a number of diagnostics have been developed with the aim of quantifying charge separation [40–44] no general solution exists yet and TDDFT is still described to suffer from "significant but hard-to-detect errors" [37]. In the following, it will be outlined how the formalism described here has potential in this context as a unified measure of static and dynamic CT effects.

A theory of exciton analysis is introduced, which relies on the sole assumption that the one-electron transition density matrix (1TDM) can be interpreted as an effective two-body exciton wave function describing the correlated *electron-hole* motion, a relation which is justified in terms of many-body Green's-function theory. Once this identification is made, there is no need for further assumptions or approximations and the exciton can be analyzed by standard quantum chemical methodology. While previous work was focused on a population analysis of this exciton wave function [25,45–48], it is in fact possible to compute expectation values with respect to any operator whose matrix elements can be evaluated

*felix.plasser@iwr.uni-heidelberg.de;
http://www.iwr.uni-heidelberg.de/groups/compchem/

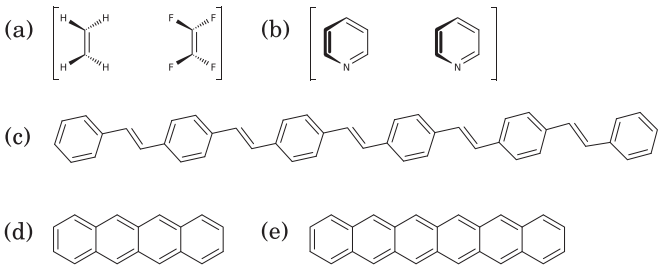

FIG. 1. Molecular systems considered in this work: (a) [ethylene tetrafluoroethylene], (b) pyridine dimer, (c) $(PV)_5P$, (d) tetracene, and (e) hexacene.

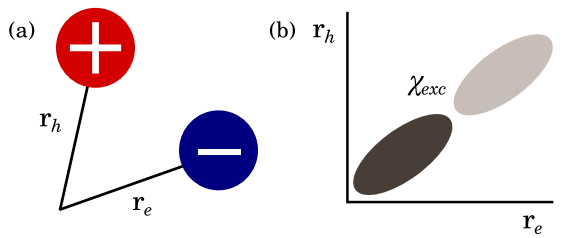

FIG. 2. (Color online) Illustration of the exciton wave function $\chi_{\mathrm{exc}}(r_h,r_e)$: (a) definition of the r_h and r_e coordinates giving the *hole* and *electron* positions; (b) schematic exciton wave function χ_{exc} with respect to these coordinates.

in the underlying orbital basis. Below, we will specifically consider the exciton size, defined as the root-mean-square (rms) *electron-hole* separation, and derive the equations to evaluate it. However, our formalism also opens a route to a wealth of other properties, e.g., binding or kinetic energies and additional spatial moments, which will be discussed in future work.

Four molecular systems are chosen to highlight different aspects of this computational protocol (Fig. 1). As a first step it is demonstrated that for simple charge-transfer states between two chromophores the newly defined exciton size is equal to their spatial distance. This is, first, explained in some detail in an analytic model and, second, the interactions of ethylene and tetrafluoroethylene ([Et$\cdots$TFE]) at varying distances are investigated for this purpose. Secondly, the symmetric pyridine dimer is selected as a representative stacked π system. In this case the differentiation between excitonic and charge resonance states in terms of the completely delocalized MOs will be illustrated (see also Refs. [46,49,50]) and different state mixing, charge separation, and excimeric effects will be discussed. Thirdly, excitons in poly (*para* phenylene vinylene) (PPV), a representative conjugated organic polymer, will be analyzed briefly. For this molecule it is of particular interest to compare the previously computed *electron-hole* correlation plots [51] with our measure of exciton size. Finally, our methodology is applied to polyacenes. In this case we want to evaluate the specific question whether our approach is able to quantify excited-state charge-transfer character even in a system where this is notoriously difficult to do [37,38].

II. EXCITON ANALYSIS

A. Basic terminology

Before starting the discussion, some of the basic quantities will be introduced and the underlying terminology will be defined (see Ref. [47] for more details). The central quantity of the presented analysis scheme, the one-particle transition density matrix (1TDM) between the ground- Φ^0 and the excited- Φ^I state wave functions, is defined as

$$\gamma^{0I}(r_h,r_e) = N \int \Phi^0(r_h,r_2,\ldots,r_N) \times \Phi^I(r_e,r_2,\ldots,r_N) dr_2,\ldots,dr_N, \quad (1)$$

where r_i denotes the spatial and spin coordinates of the ith electron: $r_i = (\vec{x}_i,s_i)$. Note that in Eq. (1) and in the following real-valued wave functions and orbitals are assumed but an extension to complex quantities is straightforward.

The matrix representation with respect to an underlying basis set of spin atomic orbitals (AOs) $\{\chi_\mu(r)\}$ is constructed as

$$D^{0I}_{\mu\nu} = \langle \Phi^0 | \hat{a}^\dagger_\mu \hat{a}_\nu | \Phi^I \rangle, \quad (2)$$

where $\hat{a}^\dagger_\mu$ and $\hat{a}_\nu$ are the creation and annihilation operators, respectively. This definition leads to an alternative expression for γ^{0I}

$$\gamma^{0I}(r_h,r_e) = \sum_{\mu\nu} D^{0I}_{\mu\nu} \chi_\mu(r_h)\chi_\nu(r_e), \quad (3)$$

which will be used in the following derivations. Finally, we note for notational convenience that

$$D^{I0}_{\nu\mu} = \langle \Phi^I | \hat{a}^\dagger_\nu \hat{a}_\mu | \Phi^0 \rangle = \langle \Phi^0 | \hat{a}^\dagger_\mu \hat{a}_\nu | \Phi^I \rangle = D^{0I}_{\mu\nu}, \quad (4)$$

i.e., switching the bra and ket states amounts to transposing the transition density matrix

$$(\mathbf{D}^{0I})^T = \mathbf{D}^{I0}. \quad (5)$$

B. Exciton wave function

As described above, some properties of excited states (e.g., exciton sizes and binding energies) are best understood in terms of a two-body exciton wave function describing the correlated motion of the *hole* and *electron* quasiparticles (cf. Fig. 2). Such a wave function appears directly within the "solid-state physics" approach of using many-body Green's-function theory [12–16,52], while it is usually not considered in the context of quantum chemistry methodology. This leads to an unfortunate gap between these two fields as far as the interpretative power of the calculations is concerned. The purpose of this section is to provide a rigorous framework to bridge this gap and to unite the quasiparticle and MO pictures.

The discussion starts with the Bethe-Salpeter equation (BSE) of the exciton, which is the standard way of solving the electronic excitation problem within Green's-function theory [12,13,15]. The solution of the BSE may be expressed as the frequency- (ω) dependent two-body correlation function [13]

$$L(r_1,r_1';r_2,r_2';\omega) = i \sum_{I\neq 0} \left[\frac{\chi^I(r_1,r_1')\chi^I(r_2',r_2)}{\omega + \Delta E^I} - \frac{\chi^I(r_2,r_2')\chi^I(r_1',r_1)}{\omega - \Delta E^I} \right], \quad (6)$$

which is closely related to the polarization propagator [53]. Here, ΔE^I denotes the excitation energy of state I and χ^I is entitled the *electron-hole* amplitude. This latter function is commonly regarded as the wave function of the *electron-hole* pair [13–16] and it is precisely the quantity of interest for the purposes of this work. It is usually given in the form [13–15]

$$\chi^I(r_e,r_h) = \sum_{vc} A^I_{vc} \psi^{QP}_v(r_h)\psi^{QP}_c(r_e) \tag{7}$$

connecting the valence (ψ^{QP}_v) and conduction (ψ^{QP}_c) quasiparticle states [54].

A rigorous connection between the BSE and explicit many-body theories, and thus between the quasiparticle and MO pictures, can be given by considering the general form of the *electron-hole* amplitudes [13]

$$\chi^I(r_e,r_h) = -\langle \Phi^0 | \hat{\psi}^\dagger(r_h)\hat{\psi}(r_e)|\Phi^I\rangle, \tag{8}$$

where the field operators $\hat{\psi}(r)$ can be expressed in the AO basis as

$$\hat{\psi}(r) = \sum_\mu \hat{a}_\mu \chi_\mu(r). \tag{9}$$

Insertion of Eq. (9) into Eq. (8) already provides the relation of interest

$$\begin{aligned}\chi^I(r_e,r_h) &= -\sum_{\mu\nu}\langle \Phi^0|\hat{a}^\dagger_\mu \hat{a}_\nu|\Phi^I\rangle \chi_\mu(r_h)\chi_\nu(r_e)\\ &= -\gamma^{0I}(r_h,r_e)\,.\end{aligned} \tag{10}$$

The exciton wave function as defined within Green's-function theory is simply the 1TDM as obtained from quantum chemical calculations. If χ^I were computed by exactly solving the BSE it contains the same information as the 1TDM between the exact many-body wave functions. Thus a rigorous starting point for further investigations is provided.

Specifically, in the notation used here and in previous work [47], we define the exciton wave function as

$$\chi_{\rm exc}(r_h,r_e) := \gamma^{0I}(r_h,r_e) = -\chi^I(r_e,r_h)\,, \tag{11}$$

i.e., there is a change in sign and an exchange of the *electron* and *hole* coordinates when compared to Ref. [13] (and the I superscript is dropped for brevity).

γ^{0I} certainly possesses the required formal properties of a wave function of two distinguishable particles (i.e., being square integrable and continuously differentiable) and is therefore amenable to the computation of operator expectation values. The expectation value of an arbitrary operator $\widehat{O}$ with respect to the exciton wave function is written as

$$\langle \widehat{O}\rangle_{\rm exc} = \frac{\langle \chi_{\rm exc}|\widehat{O}|\chi_{\rm exc}\rangle}{\langle \chi_{\rm exc}|\chi_{\rm exc}\rangle}. \tag{12}$$

To evaluate this expression we follow a similar strategy as used by Tamura *et al.* [55] for the computation of energy-transfer couplings: after writing down the equations in their explicit form they are reformulated in terms of orbital integrals.

The denominator of Eq. (12) contains the squared norm of the exciton wave function Ω, a quantity which has been used to measure the single excitation character of a transition [47,56]. By inserting the definition for $\chi_{\rm exc}$ given in Eq. (11) Ω can be rewritten as

$$\Omega = \langle \chi_{\rm exc}|\chi_{\rm exc}\rangle = \int\int \gamma^{0I}(r_h,r_e)^2 dr_h dr_e. \tag{13}$$

This quantity can be reexpressed [47] in terms of matrix elements according to Eq. (3) [and using Eq. (5) for notational brevity]

$$\Omega = {\rm tr}((\mathbf{D}^{0I})^{\rm T}\mathbf{S}\mathbf{D}^{0I}\mathbf{S}) = {\rm tr}(\mathbf{D}^{I0}\mathbf{S}\mathbf{D}^{0I}\mathbf{S}). \tag{14}$$

Here $\mathbf{S}$ denotes the AO overlap matrix with elements

$$S_{\mu\nu} = \int \chi_\mu(r)\chi_\nu(r)dr. \tag{15}$$

Furthermore, the numerator of Eq. (12) can be treated in a similar fashion

$$\langle \widehat{O}\rangle_{\rm exc} = \frac{1}{\Omega}\int\int \gamma^{0I}(r_h,r_e)\widehat{O}\gamma^{0I}(r_h,r_e)dr_h dr_e, \tag{16}$$

which after insertion of Eq. (3) leads to

$$\begin{aligned}\langle \widehat{O}\rangle_{\rm exc} = \frac{1}{\Omega}\sum_{\mu\nu}\sum_{\xi\zeta} D_{\mu\nu}D_{\xi\zeta}\\ \times\int\int \chi_\mu(r_h)\chi_\nu(r_e)\widehat{O}\chi_\xi(r_h)\chi_\zeta(r_e)dr_h dr_e.\end{aligned} \tag{17}$$

In other words, the task is reduced to a contraction of the AO integrals with the density matrices. Once the AO integrals of $\widehat{O}$ are computed, the evaluation of Eq. (17) is straightforward.

The relation can be simplified in cases where the operator is given as a product of two one-particle operators, each acting on only one of the electrons, i.e., $\widehat{O} = \widehat{P}(r_h)\widehat{Q}(r_e)$. Then Eq. (17) yields

$$\begin{aligned}\langle \widehat{P}(r_h)\widehat{Q}(r_e)\rangle_{\rm exc} = \frac{1}{\Omega}\sum_{\mu\nu}\sum_{\xi\zeta} D_{\mu\nu}D_{\xi\zeta}\int\int \chi_\mu(r_h)\chi_\nu(r_e)\\ \times\widehat{P}(r_h)\widehat{Q}(r_e)\chi_\xi(r_h)\chi_\zeta(r_e)dr_h dr_e,\end{aligned} \tag{18}$$

which can be decomposed with respect to r_h and r_e

$$\begin{aligned}= \frac{1}{\Omega}\sum_{\mu\nu}\sum_{\xi\zeta} D_{\mu\nu}D_{\xi\zeta}\int \chi_\mu(r_h)\widehat{P}(r_h)\chi_\xi(r_h)dr_h\\ \times\int \chi_\nu(r_e)\widehat{Q}(r_e)\chi_\zeta(r_e)dr_e.\end{aligned} \tag{19}$$

In matrix representation this can be rewritten as

$$= \frac{1}{\Omega}\sum_{\mu\nu}\sum_{\xi\zeta} D_{\mu\nu}D_{\xi\zeta}P_{\mu\xi}Q_{\nu\zeta}, \tag{20}$$

which, in analogy to Eq. (14), finally leads to (assuming that $\mathbf{Q}$ is a symmetric matrix)

$$\langle \widehat{P}(r_h)\widehat{Q}(r_e)\rangle_{\rm exc} = \frac{1}{\Omega}{\rm tr}(\mathbf{D}^{I0}\mathbf{P}\mathbf{D}^{0I}\mathbf{Q}). \tag{21}$$

Finally, we want to point out that for an operator, which does not explicitly act on r_h and r_e but is a simple function of these coordinates [$\widehat{O} = f(r_h,r_e)$] Eq. (16) reduces to

$$\langle f(r_h,r_e)\rangle_{\rm exc} = \frac{1}{\Omega}\int\int f(r_h,r_e)\gamma^{0I}(r_h,r_e)^2 dr_h dr_e. \tag{22}$$

If, specifically, f is a polynomial then $\langle f(r_h,r_e)\rangle_{\text{exc}}$ can be interpreted as a multipole moment of the exciton distribution function χ^2_{exc}. It is precisely these types of expressions which will appear in the following text.

C. Exciton size

In this section it will be shown how Eq. (21) can be used to derive an equation for the size of the exciton. This quantity is defined here as the root-mean-square (rms) separation between the instantaneous *electron* and *hole* positions

$$d_{\text{exc}} = \sqrt{\langle|\vec{x}_h - \vec{x}_e|^2\rangle_{\text{exc}}}. \tag{23}$$

This equation may be expanded as

$$\begin{aligned} d^2_{\text{exc}} &= \langle(\vec{x}_h - \vec{x}_e)\cdot(\vec{x}_h - \vec{x}_e)\rangle_{\text{exc}} \\ &= \langle\vec{x}_h\cdot\vec{x}_h\rangle_{\text{exc}} - 2\langle\vec{x}_h\cdot\vec{x}_e\rangle_{\text{exc}} + \langle\vec{x}_e\cdot\vec{x}_e\rangle_{\text{exc}}. \end{aligned} \tag{24}$$

Further evaluation of the dot products leads to the nine terms

$$d^2_{\text{exc}} = \sum_{\xi\in\{x,y,z\}} \left(\langle\xi_h^2\rangle_{\text{exc}} - 2\langle\xi_h\xi_e\rangle_{\text{exc}} + \langle\xi_e^2\rangle_{\text{exc}}\right), \tag{25}$$

which are simple expectation values of one-electron multipole operators. Considering Eq. (21) these can be evaluated according to

$$\langle x_h^k x_e^l\rangle_{\text{exc}} = \frac{1}{\Omega}\text{tr}\left(\mathbf{D}^{I0}\mathbf{M}_x^{(k)}\mathbf{D}^{0I}\mathbf{M}_x^{(l)}\right), \tag{26}$$

where for example $\mathbf{M}_x^{(k)}$ refers to the k-order multipole matrix for coordinate x, whose components are given as

$$M^{(k)}_{x,\mu\nu} = \int \chi_\mu(r)x^k\chi_\nu(r)dr \tag{27}$$

and specifically $\mathbf{M}_\xi^{(0)} = \mathbf{S}$ is the overlap matrix in the AO basis [Eq. (15)]. These matrices are usually readily available within quantum chemical programs and thus the task is reduced to a few matrix multiplications. The final working equation is given as

$$\begin{aligned} d^2_{\text{exc}} = \frac{1}{\Omega}\sum_{\xi\in\{x,y,z\}} &\left(\text{tr}\left(\mathbf{D}^{I0}\mathbf{M}_\xi^{(2)}\mathbf{D}^{0I}\mathbf{S}\right)\right. \\ &\left. - 2\,\text{tr}\left(\mathbf{D}^{I0}\mathbf{M}_\xi^{(1)}\mathbf{D}^{0I}\mathbf{M}_\xi^{(1)}\right) + \text{tr}\left(\mathbf{D}^{I0}\mathbf{S}\mathbf{D}^{0I}\mathbf{M}_\xi^{(2)}\right)\right). \end{aligned} \tag{28}$$

The first and third terms in this sum refer to the quadrupole moments of the *hole* $\mathbf{D}^{0I}\mathbf{S}\mathbf{D}^{I0}$ and *electron* $\mathbf{D}^{I0}\mathbf{S}\mathbf{D}^{0I}$ densities (see also Ref. [47]). The second term contains mixed dipole contributions deriving from the correlated motion of the *hole* and *electron*.

As a final note, it may be pointed out that the decomposition of the two-particle problem into matrices of one-particle operators derives from the specific definition of d_{exc} as the rms separation, a simplification which is also used in the Boys orbital localization scheme [57]. By contrast the mean absolute separation $\langle|\vec{x}_h - \vec{x}_e|\rangle_{\text{exc}}$ or the mean inverse separation $\langle 1/|\vec{x}_h - \vec{x}_e|\rangle_{\text{exc}}$ (determining the Coulomb binding energy) cannot be expressed in such a simple form.

D. Electron spin

While the above equations were given in their most general form, i.e., in terms of arbitrary spin orbitals, we briefly want to mention their practical implementation in terms of spatial orbitals. For this purpose a basis of K spatial AOs $\{\varphi_\mu, 1 \leqslant \mu \leqslant K\}$ is considered and the $2K$ spin AOs are constructed as (see, e.g., Ref. [58])

$$\chi_\mu(r) = \begin{cases} \varphi_\mu(\vec{x})\alpha(s) & : \quad \mu \leqslant K, \\ \varphi_{\mu-K}(\vec{x})\beta(s) & : \quad K < \mu \leqslant 2K. \end{cases} \tag{29}$$

Using this construction the transition density matrix between two states of the same m_S quantum number is block diagonal:

$$\mathbf{D}^{0I} = \begin{pmatrix} \mathbf{D}^{0I}_\alpha & \mathbf{0} \\ \mathbf{0} & \mathbf{D}^{0I}_\beta \end{pmatrix}. \tag{30}$$

The overlap matrix is block diagonal as well and possesses two equivalent blocks, i.e.,

$$\mathbf{S} = \begin{pmatrix} \bar{\mathbf{S}} & \mathbf{0} \\ \mathbf{0} & \bar{\mathbf{S}} \end{pmatrix}, \tag{31}$$

where $\bar{\mathbf{S}}$ is the overlap matrix between the spatial AOs. By considering Eq. (14) it now follows that

$$\begin{aligned} \Omega &= \text{tr}\begin{pmatrix} \mathbf{D}^{I0}_\alpha\bar{\mathbf{S}}\mathbf{D}^{0I}_\alpha\bar{\mathbf{S}} & \mathbf{0} \\ \mathbf{0} & \mathbf{D}^{I0}_\beta\bar{\mathbf{S}}\mathbf{D}^{0I}_\beta\bar{\mathbf{S}} \end{pmatrix} \\ &= \text{tr}\left(\mathbf{D}^{I0}_\alpha\bar{\mathbf{S}}\mathbf{D}^{0I}_\alpha\bar{\mathbf{S}}\right) + \text{tr}\left(\mathbf{D}^{I0}_\beta\bar{\mathbf{S}}\mathbf{D}^{0I}_\beta\bar{\mathbf{S}}\right) \\ &= \Omega_\alpha + \Omega_\beta, \end{aligned} \tag{32}$$

i.e., the α and β contributions to Ω can be evaluated individually. An analogous relation holds for general expectation values of spin-independent one-particle operators and Eq. (21) leads to

$$\langle\widehat{P}(r_h)\widehat{Q}(r_e)\rangle_{\text{exc}} = \frac{\text{tr}\left(\mathbf{D}^{I0}_\alpha\bar{\mathbf{P}}\mathbf{D}^{0I}_\alpha\bar{\mathbf{Q}}\right) + \text{tr}\left(\mathbf{D}^{I0}_\beta\bar{\mathbf{P}}\mathbf{D}^{0I}_\beta\bar{\mathbf{Q}}\right)}{\Omega_\alpha + \Omega_\beta}, \tag{33}$$

where $\bar{\mathbf{P}}$ and $\bar{\mathbf{Q}}$ are defined in analogy to Eq. (31).

Finally, the spin-restricted case will be discussed. In the case of a closed shell reference, it holds for spin-adapted singlet and triplet excited states that

$$\mathbf{D}^{0I}_\beta = \begin{cases} \mathbf{D}^{0I}_\alpha & : \quad \text{singlet}, \\ -\mathbf{D}^{0I}_\alpha & : \quad \text{triplet}, \end{cases} \tag{34}$$

which in both cases leads to

$$\text{tr}\left(\mathbf{D}^{I0}_\beta\bar{\mathbf{P}}\mathbf{D}^{0I}_\beta\bar{\mathbf{Q}}\right) = \text{tr}\left(\mathbf{D}^{I0}_\alpha\bar{\mathbf{P}}\mathbf{D}^{0I}_\alpha\bar{\mathbf{Q}}\right). \tag{35}$$

Consequently, Eq. (33) reduces to

$$\langle\widehat{P}(r_h)\widehat{Q}(r_e)\rangle_{\text{exc}} = \frac{\text{tr}\left(\mathbf{D}^{I0}_\alpha\bar{\mathbf{P}}\mathbf{D}^{0I}_\alpha\bar{\mathbf{Q}}\right)}{\Omega_\alpha} \tag{36}$$

and it suffices to consider only the α space explicitly.

III. COMPUTATIONAL DETAILS

All calculations were performed using the algebraic diagrammatic construction scheme for the polarization propagator [53] evaluated at second order in many-body perturbation theory [ADC(2)] [59] using a developmental version of the QChem 4.1 program package [60–62]. For the ethylene-tetrafluoroethylene complex and the pyridine dimer Dunning's cc-pVDZ basis set [63] was used. For computational efficiency in the cases of PPV and polyacene excited states the smaller

Ahlrichs SV basis set [64] was used as it was shown by previous studies that an unpolarized basis set is sufficient to provide a qualitatively correct description of these systems [51,65]. *Electron-hole* correlation plots of the Ω_{AB} matrices (see below) were created using an external program package [46,66].

The exciton size is compared to previously defined analysis methods of the exciton wave function in terms of the charge-transfer numbers Ω_{AB} [45–47]. Given two molecular fragments A and B these are defined as

$$\Omega_{AB} = \frac{1}{2}\sum_{\mu\in A}\sum_{\nu\in B}\left[(\mathbf{D}^{0I}\mathbf{S})_{\mu\nu}(\mathbf{S}\mathbf{D}^{0I})_{\mu\nu} + D^{0I}_{\mu\nu}(\mathbf{S}\mathbf{D}^{0I}\mathbf{S})_{\mu\nu}\right] \tag{37}$$

and mark the probability that, simultaneously, the *hole* is on fragment A and the *electron* on fragment B. In addition to a direct visualization of Ω_{AB} as an *electron-hole* correlation plot, the information can be compressed further [25,46]. In this work the charge-transfer ratio

$$\omega_{CT} = \frac{1}{\Omega}\sum_{A,B\neq A}\Omega_{AB} \tag{38}$$

is considered for this purpose, which counts the off-diagonal contributions of Ω_{AB}. ω_{CT} ranges from 0 to 1, where 0 corresponds to a local excitation or Frenkel exciton (with respect to the defined fragmentation scheme) and 1 denotes a completely charge separated state.

IV. APPLICATIONS

In this section a hierarchy of model systems is analyzed to expose the power of our computational protocol for a variety of applications (Fig. 1). First, the case of local and charge-transfer excitations in a dimer model system is discussed formally in some detail. Specific results are given for the simple case where the excitation process only consists of moving one point charge across a distance d to show that in this case $d_{exc} = d$. This relation is tested practically for the lowest CT state of a complex between ethylene (Et) and tetrafluorethylene (TFE). As a somewhat more extended example the stacked pyridine dimer at varying intermolecular separations is investigated. In this case the different behavior between excitonic and charge resonance states and mixing between them is analyzed. After these proof-of-principle investigations two examples displaying the potential of our methods in the case of conjugated organic molecules are presented. On the one hand, the structure of different excitons in PPV is analyzed. On the other hand, the excited states of polyacenes are investigated with the aim of elucidating otherwise hidden charge-transfer contributions in their excited states.

A. Dimer model

In this section the formal structure of the exciton analysis is discussed in some detail using an idealized dimer model. For this purpose, a system of two chromophores **1** and **2** is considered, each possessing two active orbitals (see also Refs. [46,49,50]). Chromophore **1** contains the initial orbital i (occupied in the ground state) and the final orbital f (unoccupied in the ground state), while the orbitals on **2** are denoted i' and f'. The eight limiting cases arising for singly excited states in such a situation are depicted in Fig. 3. On the one hand, four linearly independent states may be constructed as local excitations on each chromophore ($|\mathbf{1}^*\mathbf{2}\rangle = |i \to f\rangle$ and $|\mathbf{1}\mathbf{2}^*\rangle = |i' \to f'\rangle$) and charge-transfer states between them ($|\mathbf{1}^+\mathbf{2}^-\rangle = |i \to f'\rangle$ and $|\mathbf{1}^-\mathbf{2}^+\rangle = |i' \to f\rangle$). On the other hand, delocalized linear combinations of these may be constructed under resonance conditions leading to Frenkel excitonic (or excitonic resonance, σ and γ) and charge resonance states (δ and ρ).

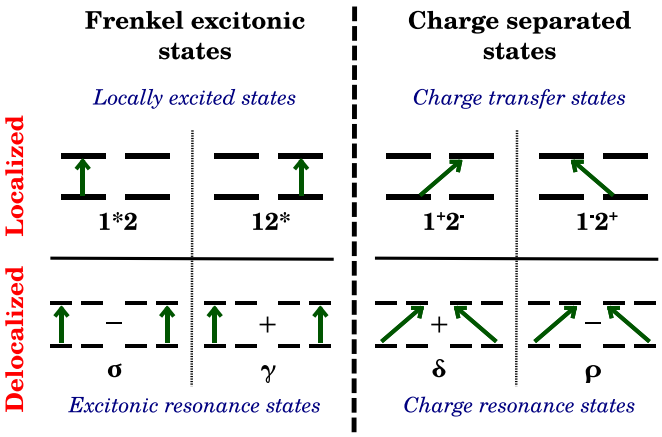

FIG. 3. (Color online) Eight limiting cases for excitation patterns emerging in the case of two chromophores with two orbitals each. Adapted from Ref. [46].

The transition density matrices $\mathbf{D}^{0I}$ arising for these states are given in Table I for the local states and Table II for the delocalized states, along with their ω_{CT} and d_{exc} values (to be discussed below). The nonzero entries of $\mathbf{D}^{0I}$ simply represent the individual orbital transitions as shown in Fig. 3.

The ω_{CT} values can be extracted immediately from Tables I and II by considering that only the off-diagonal 2×2 blocks contribute to this quantity. The locally excited and excitonic resonance states possess $\omega_{CT} = 0$, while this value is one for the charge-transfer and charge resonance states (see also Ref. [46]).

Next the analytical evaluation of Eq. (28) to compute d_{exc} will be discussed. We will first present the relevant equations in the general case and will then proceed to evaluate them with respect to a model system of pointlike orbitals. Starting with the $|\mathbf{1}^*\mathbf{2}\rangle$ state, the case of a local excitation on one molecule can be illustrated:

$$d^2_{exc}(|\mathbf{1}^*\mathbf{2}\rangle) = \sum_{\xi\in\{x,y,z\}}\left(M^{(2)}_{\xi,ii} + M^{(2)}_{\xi,ff} - 2M^{(1)}_{\xi,ii}M^{(1)}_{\xi,ff}\right). \tag{39}$$

This equation has a simple interpretation if one assumes both orbitals to be centered at the origin ($M^{(1)}_{\xi,ii} = M^{(1)}_{\xi,ff} = 0$) and to have the same spatial extent ($M^{(2)}_{\xi,ii} = M^{(2)}_{\xi,ff} = \sigma_d^2$). Then $d_{exc}(|\mathbf{1}^*\mathbf{2}\rangle) = \sigma_d\sqrt{6}$ is simply proportional to this extent.

For a charge-transfer state, e.g., $|\mathbf{1}^-\mathbf{2}^+\rangle$, an analogous equation but with respect to an altered set of orbitals is obtained:

$$d^2_{exc}(|\mathbf{1}^-\mathbf{2}^+\rangle) = \sum_{\xi\in\{x,y,z\}}\left(M^{(2)}_{\xi,ff} + M^{(2)}_{\xi,i'i'} - 2M^{(1)}_{\xi,i'i'}M^{(1)}_{\xi,ff}\right). \tag{40}$$

TABLE I. Transition density matrices[a] $\mathbf{D}^{0I}$, charge-transfer measures ω_{CT}, and exciton size d_{exc} of the idealized locally excited states $|\mathbf{1}^*\mathbf{2}\rangle$ and $|\mathbf{12}^*\rangle$ and charge-transfer states $|\mathbf{1}^-\mathbf{2}^+\rangle$ and $|\mathbf{1}^+\mathbf{2}^-\rangle$ evaluated under the assumption of a unit overlap matrix.

State	$\lvert\mathbf{1}^*\mathbf{2}\rangle$	$\lvert\mathbf{12}^*\rangle$	$\lvert\mathbf{1}^-\mathbf{2}^+\rangle$	$\lvert\mathbf{1}^+\mathbf{2}^-\rangle$
$\mathbf{D}^{0I}$	$\begin{pmatrix}0&1&0&0\\0&0&0&0\\0&0&0&0\\0&0&0&0\end{pmatrix}$	$\begin{pmatrix}0&0&0&0\\0&0&0&0\\0&0&0&1\\0&0&0&0\end{pmatrix}$	$\begin{pmatrix}0&0&0&0\\0&0&0&0\\0&1&0&0\\0&0&0&0\end{pmatrix}$	$\begin{pmatrix}0&0&0&1\\0&0&0&0\\0&0&0&0\\0&0&0&0\end{pmatrix}$
ω_{CT}	0	0	1	1
d_{exc}[b]	0	0	d	d

[a]Arranged according to (i,f,i',f').
[b]Evaluated specifically for the case of two pointlike orbitals separated by a distance d.

The equations for the delocalized states are somewhat longer but also easy to set up. For example, for the excitonic state σ one obtains

$$d^2_{\mathrm{exc}}(\sigma) = \frac{1}{2}\sum_{\xi\in\{x,y,z\}}\big(M^{(2)}_{\xi,ii} + M^{(2)}_{\xi,ff} + M^{(2)}_{\xi,i'i'} + M^{(2)}_{\xi,f'f'} - 2\big(M^{(1)}_{\xi,ii}M^{(1)}_{\xi,ff} + M^{(1)}_{\xi,i'i'}M^{(1)}_{\xi,f'f'} - 2M^{(1)}_{\xi,ii'}M^{(1)}_{\xi,ff'}\big)\big), \tag{41}$$

which includes also some matrix elements with mixed indices. A similar situation arises for the charge resonance states, e.g., for δ the exciton size is given as

$$d^2_{\mathrm{exc}}(\delta) = \frac{1}{2}\sum_{\xi\in\{x,y,z\}}\big(M^{(2)}_{\xi,ii} + M^{(2)}_{\xi,ff} + M^{(2)}_{\xi,i'i'} + M^{(2)}_{\xi,f'f'} - 2\big(M^{(1)}_{\xi,ii}M^{(1)}_{\xi,f'f'} + M^{(1)}_{\xi,ff}M^{(1)}_{\xi,i'i'} + 2M^{(1)}_{\xi,ii'}M^{(1)}_{\xi,ff'}\big)\big). \tag{42}$$

A general interpretation of the above equations can be given in the limit that the involved orbitals are points in space and that i and f, as well as i' and f', are located at the same positions, respectively. Furthermore, without loss of generality, i and f are placed at the origin of the three-dimensional coordinate system, while i' and f' are at a distance d in x direction. This leads to the multipole matrices

$$\mathbf{M}^{(k)}_x = \mathrm{diag}(0,0,d^k,d^k)\colon k \geqslant 1, \tag{43}$$

while the ones with respect to the y and z coordinates vanish. The results obtained in this way are marked as d_{exc} in Tables I and II. For locally excited states and coupled local excitations (Frenkel excitons) it holds that $d_{\mathrm{exc}} = 0$, while for the charge separated states $d_{\mathrm{exc}} = d$. In other words, d_{exc} corresponds to the natural definition of a charge-transfer distance. In the remaining sections, we will show how this concept can be extended to increasingly complex cases.

B. Ethylene tetrafluoroethylene

Previously, the stacked [Et$\cdots$TFE] complex [Fig. 1(a)] has been investigated as a prototype system for intermolecular charge transfer [31]. In this work this system is reused as a first proof-of-principle application of our approach. For this purpose, Et and TFE were set up in a parallel face-to-face arrangement using varying molecular distances between 10 and 50 Å. To compare properties of local and charge-transfer excited states, the two lowest-lying local $\pi\pi^*$ excitations on each molecule (denoted [Et$^*\cdots$TFE] and [Et$\cdots$TFE*]) and the CT state from Et to TFE [Et$^+\cdots$TFE$^-$] are investigated at the ADC(2)/cc-pVDZ level of theory.

The excitation energies and exciton sizes d_{exc} of these three states are presented in Fig. 4. For the local states (positioned at S_2 and S_3) the excitation energies remain constant at about 8.73 and 8.77 eV for the range considered. By contrast the energy of the CT state increases strongly according to the expected $1/d$ behavior (where d is the intermolecular separation), which follows from the electrostatic attraction between the *electron* and the *hole*. Accordingly, the relative position of this state is somewhat raised: while it is the S_{12} state at $d = 10$ Å, it becomes the S_{14} state at $d = 50$ Å. Similar to the excitation energies also the exciton sizes of the local states remain constant at $d_{\mathrm{exc}} = 1.94$ and 2.04 Å for [Et$^*\cdots$TFE] and [Et$\cdots$TFE*], respectively [Fig. 4(b)]. These values are identical to the ones for the $\pi\pi^*$ states of the isolated Et and TFE molecules. For the CT state there is a close correspondence between d and d_{exc} and only a minor difference remains due to the nonvanishing size of the molecules making d_{exc} somewhat larger. For example, at a distance of $d = 10$

TABLE II. Transition density matrices[a] $\mathbf{D}^{0I}$, charge-transfer measures ω_{CT}, and exciton size d_{exc} of the idealized Frenkel excitonic resonance states σ and γ and charge resonance states δ and ρ evaluated under the assumption of a unit overlap matrix.

State	σ	γ	δ	ρ
$\mathbf{D}^{0I}\cdot\sqrt{2}$	$\begin{pmatrix}0&1&0&0\\0&0&0&0\\0&0&0&-1\\0&0&0&0\end{pmatrix}$	$\begin{pmatrix}0&1&0&0\\0&0&0&0\\0&0&0&1\\0&0&0&0\end{pmatrix}$	$\begin{pmatrix}0&0&0&1\\0&0&0&0\\0&1&0&0\\0&0&0&0\end{pmatrix}$	$\begin{pmatrix}0&0&0&1\\0&0&0&0\\0&-1&0&0\\0&0&0&0\end{pmatrix}$
ω_{CT}	0	0	1	1
d_{exc}[b]	0	0	d	d

[a]Arranged according to (i,f,i',f').
[b]Evaluated specifically for the case of two pointlike orbitals separated by a distance d.

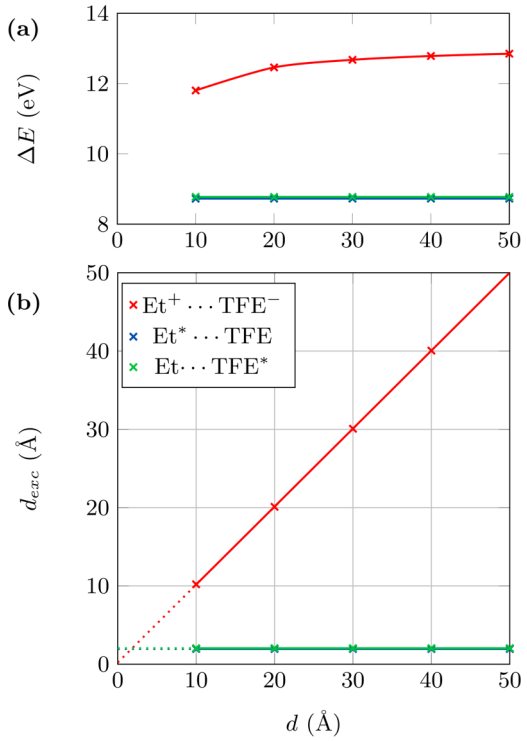

FIG. 4. (Color online) (a) Excitation energies of charge transfer and locally excited $\pi\pi^*$ states of [Et$\cdots$TFE] and (b) exciton sizes (d_{exc}, Å) examined for varied molecular separations d (Å) at the ADC(2)/cc-pVDZ level of theory.

Å the exciton size is 10.20 Å. In summary, the results are consistent with the theoretical considerations of the previous section and highlight the suitability of d_{exc} for quantifying charge transfer.

C. Pyridine dimer

Complexes of aromatic and heteroaromatic molecules are highly interesting models for biological chromophores with particular relevance to DNA [67]. The excited states of these systems are characterized by excitonic delocalization and charge transfer, and at smaller intermolecular separations exciplex interactions come into play [68,69]. However, analyzing these processes is challenging, in particular when several transitions between delocalized orbitals are involved [46,50]. The pyridine dimer [70,71] is chosen here as a prototypical example: two pyridine molecules are positioned in a face-to-face arrangement, with the nitrogen atoms located on top of each other yielding C_{2v} symmetry for the total system. Due to this symmetric arrangement, all states and MOs are evenly delocalized over the system and no net charge transfer or dipole moments are present. While this is a challenging situation for standard analysis methods [50,72], the states can be readily characterized using the charge-transfer measure ω_{CT} and exciton size d_{exc} as defined above.

In Table III a summary of the 15 lowest-lying singlet states of the pyridine dimer at 5 Å distance is presented. The twelve lowest-lying states are excitonic resonance states of $n\pi^*$ and $\pi\pi^*$ nature. These states arise as the σ and γ linear combinations (cf. Fig. 3) of the six low-lying states of the

TABLE III. Excitation energies (ΔE, eV), oscillator strengths (f), charge-transfer measures (ω_{CT}), exciton sizes (d_{exc}, Å), and type assignment of the 15 lowest-energy singlet $n\pi^*$, $\pi\pi^*$, CT, and Rydberg states of the pyridine dimer at an intermolecular separation of 5 Å at the ADC(2)/cc-pVDZ level of theory.

State	ΔE	f	ω_{CT}	d_{exc}	Type
$1\,^1B_1$	5.13	0.00	0.000	2.55	$n\pi^*$
$2\,^1A_1$	5.13	0.00	0.000	2.55	$n\pi^*$
$1\,^1A_2$	5.37	0.00	0.000	2.57	$n\pi^*$
$1\,^1B_2$	5.37	0.00	0.000	2.57	$n\pi^*$
$2\,^1A_2$	5.44	0.00	0.001	2.43	$\pi\pi^*$
$2\,^1B_2$	5.45	0.04	0.000	2.43	$\pi\pi^*$
$2\,^1B_1$	6.92	0.00	0.002	2.54	$\pi\pi^*$
$3\,^1A_1$	6.95	0.04	0.000	2.53	$\pi\pi^*$
$3\,^1A_2$	7.67	0.00	0.006	2.51	$\pi\pi^*$
$3\,^1B_1$	7.78	0.00	0.005	2.57	$\pi\pi^*$
$3\,^1B_2$	7.84	1.10	0.000	2.49	$\pi\pi^*$
$4\,^1A_1$	7.92	0.92	0.008	2.72	$\pi\pi^*$
$4\,^1B_1$	8.00	0.00	0.990	5.65	$n\pi^*$
$5\,^1A_1$	8.00	0.02	0.984	5.63	$n\pi^*$
$5\,^1B_1$	8.19	0.00	0.011	3.81	Rydberg

pyridine monomer [48,73]. In all these cases ω_{CT} is very close to zero and the exciton size is about 2.5 Å. After these twelve excitonic states, the two charge separated states ($\omega_{\text{CT}} \approx 0.99$) $4\,^1B_1$ and $5\,^1A_1$ follow. Their exciton sizes ($d_{\text{exc}} \approx 5.6$ Å) reflect the extended *electron-hole* separation of these states spanning the intermolecular separation of 5.0 Å. These are the δ and ρ charge resonance states deriving from the same orbitals as the $1\,^1B_1$ and $2\,^1A_1$, σ and γ excitonic states, forming together a complete set of four delocalized states as described in Fig. 3. The last state considered is the $5\,^1B_1$ state. This state is local in the sense that $\omega_{\text{CT}} \approx 0.0$, but Table III reveals that its exciton size is somewhat increased compared to the previous cases ($d_{\text{exc}} = 3.81$ Å). The reason for this is the Rydberg character of this state, i.e., the diffuse *particle* orbital leads to an increase of the exciton size.

Table III is used as a starting point for a scan of intermolecular separations between 2.5 and 9 Å. To reduce the complexity of the information only states of B_1 symmetry will be considered, as this irreducible representation contains both the lowest-lying excitonic and charge resonance states. In Fig. 5 the relative energies, exciton sizes d_{exc}, and the ω_{CT} values of these states are plotted against the intermolecular separation.

Above separations of 6.0 Å (i.e., on the right-hand side of Fig. 5) the first three excited states ($1\,^1B_1$–$3\,^1B_1$) are excitonic combinations of $n\pi^*$ and $\pi\pi^*$ states, while $4\,^1B_1$ is a Rydberg state and none of these states show any charge separation ($\omega_{\text{CT}} = 0$). The $n\pi^*$ charge resonance state ($\omega_{\text{CT}} = 1$) is the highest-lying state presented here ($5\,^1B_1$). This latter state exhibits the expected $1/d$ dependence of the total energy and a linear growth of d_{exc} comparable to the CT state [Et$^+\cdots$TFE$^-$] described previously. For the other states these values remain constant possessing similar values as in Table III. In Fig. 5, coming from the right, the first state crossing occurs at about 5.75 Å affecting the Rydberg and the charge resonance state. This goes along with an abrupt exchange of the excited-state

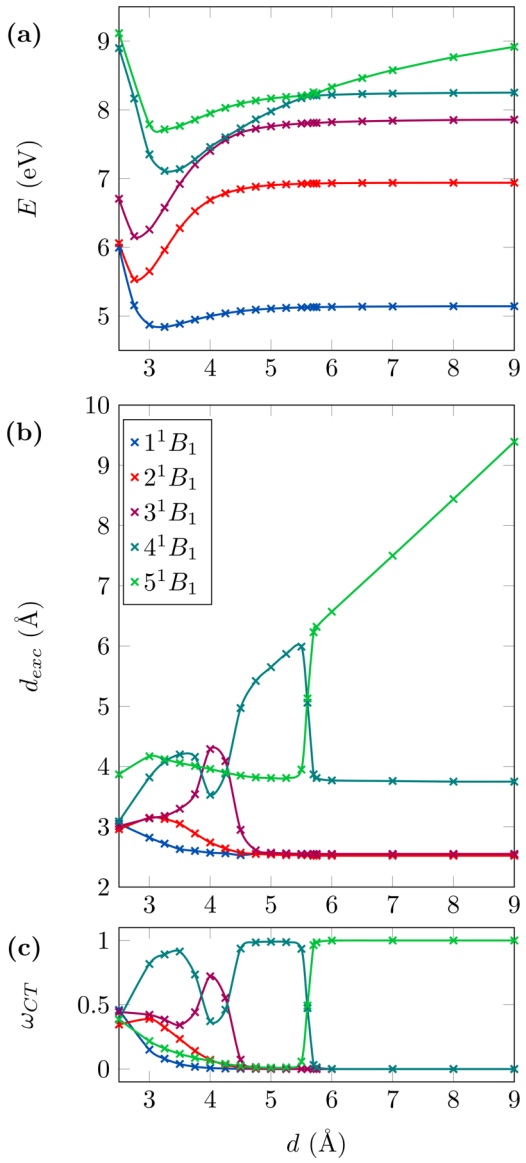

FIG. 5. (Color online) (a) Total energies relative to the ground state at infinite separation (E, eV), (b) exciton sizes (d_{exc}, Å), and (c) charge-transfer measures (ω_{CT}) for the five energetically lowest-lying $^1B_1$ states of pyridine dimer calculated at the ADC(2)/cc-pVDZ level for varied molecular separations d (Å).

characters of the $4\,^1B_1$ and $5\,^1B_1$ states as seen in Figs. 5(b) and 5(c).

Below about 5 Å direct orbital interactions come into play [50] and the clear distinction between excitonic and charge resonance states is no longer possible. In Fig. 5 this effect can be seen by the fact that starting at around this separation the d_{exc} and ω_{CT} values of the individual states diverge from the idealized results described above. This effect is enhanced for the $3\,^1B_1$ and the $4\,^1B_1$ states which lie close in energy over an extended geometric range around $d = 4$ Å. Substantial coupling between these states leads to strong modulations of the d_{exc} and ω_{CT} values.

At intermolecular separations below 3.5 Å excimeric effects play the dominant role. In particular, the $\pi\pi^*$ states ($2\,^1B_1$ and the $3\,^1B_1$) exhibit deep potential wells at intermolecular separations below 3.0 Å. It should be noted that a quantitatively correct description of these minima cannot be guaranteed using the present computational protocol owing to potential multireference effects and basis set superposition error [69], but a semiquantitative analysis of the wave functions is certainly of highest interest. As discussed previously [46,67,69], the energetic stabilization goes along with a significant change in wave-function character, which is reflected by the fact that at smaller separations the charge-transfer measures (ω_{CT}) of all states approach a value of 0.5. This means that the differentiation between excitonic and charge separated states disappears and the resulting exciplex states are of a homogeneous and coherent nature. An analogous trend is also observed for d_{exc}, which converges to about 3.0 Å for all the valence states. Only the Rydberg state ($4\,^1B_1$) retains its distinctly higher value of 3.87 Å. In summary, it could be shown that the presented analysis strategy is indeed useful for drawing a detailed picture about excited-state characters in stacked systems and that new quantitative information can be provided, which remains hidden when applying simpler analysis strategies.

D. Poly(para phenylene vinylene)

Over the past decades the study of poly(*para* phenylene vinylene) has provided fundamental insight into the working principles of π-conjugated polymers used in organic electronics [1,11,28]. However, a number of questions remain open and especially the magnitude of the exciton binding energy is still discussed controversially [8,74–78]. Aside from the large system sizes the main barrier for computational studies lies in the fact that even when accurate excitation energies are available, an analysis of excitonic correlation effects is by far not trivial and outside the scope of standard quantum chemical approaches. One strategy used to overcome these problems is the analysis of the 1TDM, which could indeed reveal otherwise hidden excitonic properties [17,25,51]. In this work, the idea is moved forward and quantitative information is gained through the analysis of exciton sizes.

For the description of PPV we revisit the strategies explored in Refs. [46,51]. The main previous tool in this context are the charge-transfer numbers Ω_{AB} [Eq. (37)] [45,46], which can be used to represent the correlated *electron-hole* distribution in a graphical manner (see also Refs. [7,23,25,79]). To perform this analysis, the system is first divided into "chemically intuitive" fragments and then the Ω_{AB} are used to encode the joint probability of finding the *hole* and *electron* at fragments A and B, respectively. A matrix pseudocolor plot of this quantity is used to visualize the correlated *electron-hole* wave function in a representation corresponding to Fig. 2(b), i.e., the *hole* and *electron* positions are plotted along the horizontal and vertical axis, respectively. Elements on the main diagonal represent local excitations within one fragment, whereas charge-transfer contributions between two fragments can be found as off-diagonal elements. While the CT numbers are indeed useful for representing excitonic structures in conjugated organic polymers, there are several downsides. The results depend on the fragment definitions and population analysis scheme chosen, and the plots are only easily interpreted for linear

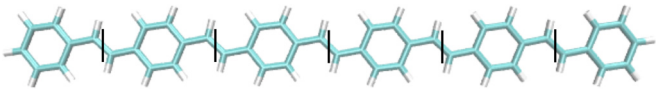

FIG. 6. (Color online) Fragmentation scheme for Ω_{AB} plots of $(PV)_5P$.

molecules. To overcome these problems, we employ the exciton size d_{exc} as a more compact and clearly defined descriptor of *electron-hole* separation.

A hexamer fragment of poly(*para* phenylene vinylene) termed $(PV)_5P$ was considered as a model for the spectroscopic unit in the polymer. To perform the CT number analysis, the molecule was split into six quasiequivalent fragments by cutting through carbon-carbon double bonds (Fig. 6; see also Refs. [46,51]). The resulting correlation plots and additional pieces of information of the lowest four singlet and triplet excited states of $(PV)_5P$ are presented in Table IV.

A first visual inspection of the correlation plots for the singlet excited states directly suggests the existence of two distinct excitation patterns: the first three states (S_1–S_3) resemble a series of particle-in-a-box-like excitations with increasing number of nodes subdividing the π system into regular units (see also Ref. [18]). By contrast, the S_4 state ($3\,^1A_g$) has much more pronounced off-diagonal contributions highlighting its enhanced intrinsic charge-transfer character. The same trend can also be seen in the ω_{CT} values [counting the fraction of charge separated configurations in the excited state, Eq. (38)]. For the first three states ω_{CT} stays between 0.61 and 0.51 getting somewhat lower for the higher excited states, while the value of $\omega_{CT} = 0.75$ for S_4 indicates a considerable charge separation (according to the fragmentation scheme chosen).

In Table IV also the exciton size d_{exc} is presented, which allows for a more quantitative comparison among the states. The sizes for the first three states are somewhat smaller than the length of the PV repeat unit (6.71 Å), while being significantly larger than the diameter of a single phenyl ring (2.86 Å) [see Ref. [19] for a related analysis in poly(*para* phenylene)].

TABLE IV. Excitation energies (ΔE, eV), exciton sizes (d_{exc}, Å), charge-transfer measures (ω_{CT}), and *electron-hole* pair-correlation plots Ω_{AB} of the first four singlet and triplet excited states of $(PV)_5P$ computed at the ADC(2)/SV level.

	$S_1(1^1B_u)$	$S_2(2^1A_g)$	$S_3(2^1B_u)$	$S_4(3^1A_g)$
ΔE	3.45	3.96	4.46	4.50
d_{exc}	6.49	5.92	5.19	10.45
ω_{CT}	0.61	0.59	0.51	0.75
Ω_{AB}				
	$T_1(1^3B_u)$	$T_2(1^3A_g)$	$T_3(2^3B_u)$	$T_4(2^3A_g)$
ΔE	2.28	2.49	2.78	3.12
d_{exc}	4.53	4.14	3.79	3.47
ω_{CT}	0.38	0.36	0.34	0.32
Ω_{AB}				

These values are in agreement with the Ω_{AB} plots showing that excitations occur either locally or between adjacent fragments. With an increase of nodes perpendicular to the π system, the *electron-hole* distance d_{exc} drops from 6.49 to 5.19 Å meaning that the exciton becomes somewhat more tightly bound for the higher momentum particle-in-a-box states (a similar trend is observed in Ref. [17]). In comparison to the (S_1–S_3) states the *electron-hole* separation of S_4 is much larger with $d_{exc} = 10.45$ Å. Previous studies [46,51] suggested the S_4 state to belong to a distinct PPV band and the difference in d_{exc} is in agreement with this idea (see also Ref. [10] for a discussion of the different possible states).

For all four triplet states exciton patterns similar to the S_1–S_3 state series can be found. The *electron-hole* correlation plots suggest a series of particle-in-a-box-like excitations. However, in contrast to the singlet states, the triplets show a reduced CT character (see also Ref. [17]). Accordingly, the mean *electron-hole* distances are significantly smaller lying between 4.53 and 3.47 Å. These findings nicely reflect the contrasting exchange-correlation effects expected for singlet and triplet excitons [11] as only the former are affected by exchange repulsion between the *electron* and the *hole*.

E. Polyacenes

Polyacenes are a promising substance class for applications in organic electronics due to their unique electronic structure properties. However, the description of their electronic states is quite challenging [35,37,65,80–83]. In particular, in the case of the larger polyacenes open-shell character in the ground state [80] and doubly excited character in some of the excited states come into play [81]. Furthermore, there are specific problems for TDDFT even at smaller system sizes [35,37]. In light of these considerations a more detailed understanding of polyacene excited states is certainly of highest interest. This work is specifically concerned with the tetracene and hexacene molecules, which have comparatively large π systems but are still amenable to a single reference approach [80].

The two lowest spectroscopically relevant states, usually termed $^1L_a(1\,^1B_{2u})$ and $^1L_b(1\,^1B_{3u})$, are computed at the ADC(2) level (which has been tested for this purpose previously [81]). To analyze the general character of these states, we first consider the transition densities and moments in the case of tetracene (Fig. 7). In this representation it can be seen that the ^1L_a state is polarized along the short axis (the transition moment points in this direction) and possesses a large oscillator strength ($f = 0.113$). By contrast, the ^1L_b state is polarized along the long axis and is almost dark ($f = 0.002$). The transition density is located on the carbon atoms for the ^1L_a state while it is centered around the bonds in the ^1L_b case (see also Ref. [37]).

To get more insight into the wave functions of these states a similar strategy as in Sec. IV D is adopted, i.e., a decomposition in terms of charge-transfer numbers as well as the computation of d_{exc}. However, in contrast to $(PV)_5P$ setting up the fragmentation scheme needed for the charge-transfer analysis is not quite as unambiguous. The choice finally adopted is presented in Fig. 8. Unfortunately, it is not possible to set up chemically equivalent fragments in this way and the obtained results should be analyzed with care. By contrast,

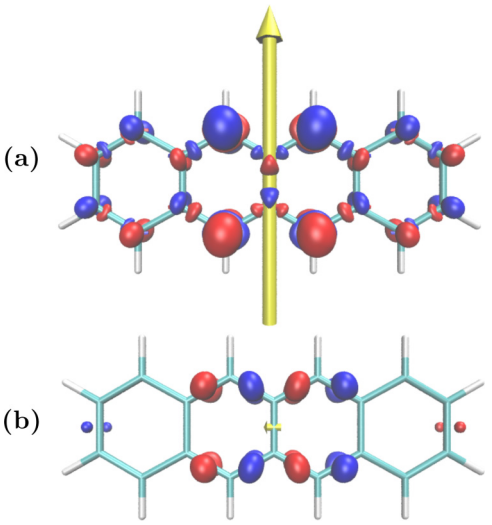

FIG. 7. (Color online) Transition densities (with isovalue 0.003e) and transition moments shown as yellow arrows with volume proportional to the oscillator strength for (a) the ^1L_a and (b) the ^1L_b state of tetracene.

there is no such arbitrariness in the computation of d_{exc}, which highlights the power of this approach. The results of this investigation are presented in Table V. For both systems the ^1L_a state is significantly lower in energy than the ^1L_b state and possesses by far the larger oscillator strength. An inspection of the *electron-hole* pair-correlation plots (Ω_{AB}) reveals clear differences between the states. The ^1L_a state possesses enhanced charge separation (strong contributions on the upper left and lower right corners) and notably no contribution on the central fragment. By contrast, the ^1L_b states possess enhanced contributions on the main diagonal (going from lower left to upper right), which derive from configurations where the *electron* and *hole* are on the same fragment. While the construction and interpretation of these correlation plots is quite involved, d_{exc} provides a more compact and simple descriptor of the dynamical charge transfer in these systems. Two trends can be seen immediately. First, d_{exc} increases when going from tetracene to hexacene, meaning that there is a significant change in electronic structure between these molecules, which probably derives from confinement effects. Second, in both cases the charge separation for the ^1L_a state is significantly larger when compared to the ^1L_b state.

Interestingly, it has been known for a long time that the ^1L_a state of polyacenes is not described well by local

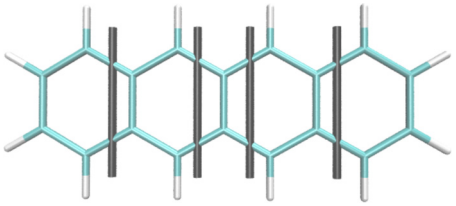

FIG. 8. (Color online) Fragmentation scheme for *electron-hole* pair-correlation plots Ω_{AB} for tetracene. Hexacene is fragmented in analogy.

TABLE V. Excitation energies (ΔE, eV) with oscillator strengths in parentheses, exciton sizes (d_{exc}, Å), and *electron-hole* pair-correlation plots (Ω_{AB}) of tetracene and hexacene excited states computed at the ADC(2)/SV level of theory.

Tetracene	^1L_a	^1L_b
ΔE	3.20(0.113)	3.67(0.002)
d_{exc}	4.60	4.02
Ω_{AB}		
Hexacene	^1L_a	^1L_b
ΔE	2.18(0.093)	3.23(0.006)
d_{exc}	5.60	4.76
Ω_{AB}	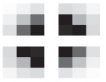	

density functionals [35]. This phenomenon, which has been attributed to hidden charge transfer, has since been difficult to understand in a quantitative sense [37,38]. However, the presented results show that d_{exc} does indeed find enhanced charge transfer for this state. Combined with the results of the previous sections, discussing charge separation in dimers, these findings suggest that d_{exc} carries potential as a general charge-transfer diagnostic for TDDFT (see Refs. [40–44] for alternative strategies). The present formalism is certainly extensible to TDDFT, using for example Casida's construction of an approximate 1TDM [84], but to judge the full power of this approach a more detailed investigation is needed including most importantly an implementation at the TDDFT level.

V. CONCLUSIONS

The purpose of this work was to define and implement a tool for excited-state analysis in the quest to bridge a gap between quantum chemistry and solid-state physics as far as the phenomenology of excited states is concerned. The essence of our approach is a mapping between the molecular orbital and quasiparticle pictures, which is achieved through identifying the one-particle transition density matrix of a many-body quantum chemical calculation with an effective exciton wave function. Once this identification is made, properties of the exciton are readily available using standard quantum chemical methodology. The exciton size or dynamic charge-transfer character is considered here as a highly interesting and at the same time easily accessible property. The equations were implemented within the *ab initio* ADC scheme, and an extension to any method providing transition density matrices is readily achieved.

We expect that our approach can provide important insight for calculations of dimers and aggregates as well as of extended π-conjugated systems. Three examples of the first class were chosen: (i) an analytical dimer model of two separated chromophores, (ii) the ethylene tetrafluoroethylene system, and (iii) the pyridine dimer. The main result of this investigation is that in the case of charge-transfer and charge resonance states an almost perfect correspondence between the

exciton size and the intermolecular separation is found, while for local and Frenkel excitonic states the exciton size depends only on the monomer properties. Furthermore, in the case of the pyridine dimer state mixing, orbital interactions, and excimeric effects could be readily analyzed using our methods. This example also revealed that Rydberg states possess high d_{exc} values and a differentiation between these and charge separated valence states is only possible when considering additional properties, as described above.

The second class of molecular systems where our analysis strategy has great potential are large extended π systems. In this context PPV and polyacenes were examined. In both cases it could be shown that a wealth of information could be recovered, which would remain hidden if only the Hartree-Fock orbitals were analyzed. The outcome was compared to the literature, finding good agreement with a variety of results and hypotheses by other researchers. Specifically, the new exciton size measure proved beneficial with respect to the analysis of dynamic charge separation effects providing a more compact quantitative measure when compared to previously used *electron-hole* correlation plots [25,51].

Aside from the purpose of extracting physical information out of quantum chemical calculations, there is also an interesting methodological component to our method: owing to the failure of standard density functionals in the description of charge-transfer states [31] there is an ongoing quest for at least providing a reliable and general diagnostic to identify charge-transfer interactions [40–44]. In this work it was shown (i) that d_{exc} provides the expected charge separation distance for directed charge-transfer states, (ii) that it identifies charge resonance states in symmetric systems, and (iii) that, even more, dynamic charge-transfer contributions in conjugated organic polymers can be quantified, which is a notoriously difficult problem [37,38]. An implementation of the exciton size within a TDDFT framework is on its way to evaluate its utility in more detail.

The presented approach may be readily extended to further properties of exciton wave functions. Different spatial moments of the *electron*, the *hole*, or the combined wave function may be directly evaluated in analogy to Sec. II C. This could provide a wealth of new information going from simple measures like the extent of the *hole* and *particle* densities (allowing, e.g., the characterization of Rydberg states) to more extended ideas like the quantification of spatial correlation. Going beyond spatial moments, the methodology is also amenable to energetic properties by considering the electron repulsion (for computing binding energies) and kinetic-energy operators.

ACKNOWLEDGMENTS

S.A.B. acknowledges funding of the Heidelberg Graduate School of Mathematical and Computational Methods for the Sciences, University of Heidelberg. F.P. acknowledges the support received from an Alexander von Humboldt-Stiftung fellowship.

[1] J.-L. Bredas, J. Cornil, D. Beljonne, D. A. Dos Santos, and Z. Shuai, Acc. Chem. Res. **32**, 267 (1999).
[2] F. Plasser, M. Barbatti, A. J. A. Aquino, and H. Lischka, Theor. Chem. Acc. **131**, 1073 (2012).
[3] D. Lumpi, E. Horkel, F. Plasser, H. Lischka, and J. Fröhlich, Chem. Phys. Chem. **14**, 1016 (2013).
[4] H. Tamura and I. Burghardt, J. Am. Chem. Soc. **135**, 16364 (2013).
[5] R. Tautz, E. Da Como, C. Wiebeler, G. Soavi, I. Dumsch, N. Fröhlich, G. Grancini, S. Allard, U. Scherf, G. Cerullo, S. Schumacher, and J. Feldmann, J. Am. Chem. Soc. **135**, 4282 (2013).
[6] H. Li, R. Nieman, A. J. A. Aquino, H. Lischka, and S. Tretiak, J. Chem. Theor. Comput. **10**, 3280 (2014).
[7] I. G. Scheblykin, A. Yartsev, T. Pullerits, V. Gulbinas, and V. Sundström, J. Phys. Chem. B **111**, 6303 (2007).
[8] T. M. Clarke and J. R. Durrant, Chem. Rev. **110**, 6736 (2010).
[9] M. Kuik, G.-J. A. H. Wetzelaer, H. T. Nicolai, N. I. Craciun, D. M. De Leeuw, and P. W. M. Blom, Adv. Mater. **26**, 512 (2014).
[10] W. Barford, J. Phys. Chem. A **117**, 2665 (2013).
[11] N. Kirova, Polym. Int. **57**, 678 (2008).
[12] G. Strinati, Phys. Rev. B **29**, 5718 (1984).
[13] M. Rohlfing and S. G. Louie, Phys. Rev. B **62**, 4927 (2000).
[14] J.-W. van der Horst, P. A. Bobbert, M. A. J. Michels, and H. Bässler, J. Chem. Phys. **114**, 6950 (2001).
[15] G. Onida, L. Reining, and A. Rubio, Rev. Mod. Phys. **74**, 601 (2002).
[16] T. G. Pedersen and T. B. Lynge, Comput. Mater. Sci. **27**, 123 (2003).
[17] A. V. Luzanov, J. Struct. Chem. **43**, 711 (2002).
[18] J. Rissler, Chem. Phys. Lett. **395**, 92 (2004).
[19] W. Barford and N. Paiboonvorachat, J. Chem. Phys. **129**, 164716 (2008).
[20] H. Ma, T. Qin, and A. Troisi, J. Chem. Theor. Comput. **10**, 1272 (2014).
[21] P. K. Nayak, Synth. Met. **174**, 42 (2013).
[22] Z.-H. Yang and C. A. Ullrich, Phys. Rev. B **87**, 195204 (2013).
[23] E. Zojer, P. Buchacher, F. Wudl, J. Cornil, J. P. Calbert, J. L. Brédas, and G. Leising, J. Chem. Phys. **113**, 10002 (2000).
[24] J. Rissler, H. Bässler, F. Gebhard, and P. Schwerdtfeger, Phys. Rev. B **64**, 045122 (2001).
[25] S. Tretiak and S. Mukamel, Chem. Rev. **102**, 3171 (2002).
[26] C. De Leener, E. Hennebicq, J.-C. Sancho-Garcia, and D. Beljonne, J. Phys. Chem. B **113**, 1311 (2009).
[27] It is indeed possible to define various kinds of population analyses within this theory but these are not a required input.
[28] G. D. Scholes and G. Rumbles, Nat. Mater. **5**, 683 (2006).
[29] S. Sharifzadeh, P. Darancet, L. Kronik, and J. B. Neaton, J. Phys. Chem. Lett. **4**, 2197 (2013).
[30] H. M. Heitzer, B. M. Savoie, T. J. Marks, and M. A. Ratner, Ang. Chem. Int. Ed. **53**, 1 (2014).
[31] A. Dreuw, J. L. Weisman, and M. Head-Gordon, J. Chem. Phys. **119**, 2943 (2003).
[32] A. Dreuw and M. Head-Gordon, J. Am. Chem. Soc. **126**, 4007 (2004).
[33] S. Tretiak, K. Igumenshchev, and V. Chernyak, Phys. Rev. B **71**, 033201 (2005).

[34] Z. L. Cai, K. Sendt, and J. R. Reimers, J. Chem. Phys. **117**, 5543 (2002).

[35] S. Grimme and M. Parac, Chem. Phys. Chem. **4**, 292 (2003).

[36] V. Lukes, A. J. A. Aquino, H. Lischka, and H.-F. Kauffmann, J. Phys. Chem. B **111**, 7954 (2007).

[37] R. Richard and J. Herbert, J. Chem. Theor. Comput. **7**, 1296 (2011).

[38] N. Kuritz, T. Stein, R. Baer, and L. Kronik, J. Chem. Theor. Comput. **7**, 2408 (2011).

[39] D. Lumpi, E. Horkel, F. Plasser, H. Lischka, and J. Fröhlich, Chem. Phys. Chem. **14**, 1016 (2013).

[40] M. J. G. Peach, P. Benfield, T. Helgaker, and D. J. Tozer, J. Chem. Phys. **128**, 044118 (2008).

[41] T. Le Bahers, C. Adamo, and I. Ciofini, J. Chem. Theor. Comput. **7**, 2498 (2011).

[42] C. A. Guido, P. Cortona, B. Mennucci, and C. Adamo, J. Chem. Theor. Comput. **9**, 3118 (2013).

[43] C. A. Guido, P. Cortona, and C. Adamo, J. Chem. Phys. **140**, 104101 (2014).

[44] T. Etienne, X. Assfeld, and A. Monari, J. Chem. Theor. Comput. **10**, 3906 (2014).

[45] A. V. Luzanov and O. A. Zhikol, Int. J. Quantum Chem. **110**, 902 (2010).

[46] F. Plasser and H. Lischka, J. Chem. Theor. Comput. **8**, 2777 (2012).

[47] F. Plasser, M. Wormit, and A. Dreuw, J. Chem. Phys. **141**, 024106 (2014).

[48] F. Plasser, S. Bäppler, M. Wormit, and A. Dreuw, J. Chem. Phys. **141**, 024107 (2014).

[49] G. D. Scholes and K. P. Ghiggino, J. Phys. Chem. **98**, 4580 (1994).

[50] A. L. L. East and E. C. Lim, J. Chem. Phys. **113**, 8981 (2000).

[51] A. N. Panda, F. Plasser, A. J. A. Aquino, I. Burghardt, and H. Lischka, J. Phys. Chem. A **117**, 2181 (2013).

[52] C. Faber, I. Duchemin, T. Deutsch, and X. Blase, Phys. Rev. B **86**, 155315 (2012).

[53] J. Schirmer, Phys. Rev. A **26**, 2395 (1982).

[54] Note that in Eq. (7) two distinct sets of valence and conduction states appear, while in Eq. (3) both indices run over the whole set of atomic orbitals. The former simplification follows from the specific form of Eq. (6) and the Tamm-Dancoff approximation (see also Ref. [13]).

[55] H. Tamura, J. M. Mallet, M. Oheim, and I. Burghardt, J. Phys. Chem. C **113**, 7548 (2009).

[56] S. Matsika, X. Feng, A. V. Luzanov, and A. I. Krylov, J. Phys. Chem. A (2014), doi:10.1021/jp506090g.

[57] S. F. Boys, in *Quantum Theory of Atoms, Molecules and the Solid State*, edited by P. O. Löwdin (Academic Press, New York, 1968).

[58] A. Szabo and N. S. Ostlund, *Modern Quantum Chemistry–Introduction to Advanced Electronic Structure Theory* (Dover, Mineola, NY, 1996).

[59] A. B. Trofimov and J. Schirmer, J. Phys. B **28**, 2299 (1995).

[60] Y. Shao, L. F. Molnar, Y. Jung, J. Kussmann, C. Ochsenfeld, S. T. Brown, A. T. Gilbert, L. V. Slipchenko, S. V. Levchenko, D. P. O'Neill, R. A. DiStasio, Jr., R. C. Lochan, T. Wang, G. J. Beran, N. A. Besley, J. M. Herbert, C. Yeh Lin, T. Van Voorhis, S. Hung Chien, A. Sodt, R. P. Steele, V. A. Rassolov, P. E. Malsen, P. P. Korambath, R. D. Adamson, B. Austin, J. Baker, E. F. C. Byrd, H. Dachsel, R. J. Doerksen, A. Dreuw, B. D. Dunietz, A. D. Dutoi, T. R. Furlani, S. R. Gwaltney, A. Heyden, S. Hirata, C.-P. Hsu, G. Kedziora, R. Z. Khalliulin, P. Klunzinger, A. M. Lee, W. Liang, I. Lotan, N. Nair, B. Peters, E. I. Proynov, P. A. Pieniazek, Y. Min Rhee, J. Ritchie, E. Rosta, C. David Sherrill, A. C. Simmonett, J. E. Subotnik, H. Lee Woodcock III, W. Zhang, A. T. Bell, A. K. Chakraborty, D. M. Chipman, F. J. Keil, A. Warshel, W. J. Hehre, H. F. Schaefer III, J. Kong, A. I. Krylov, P. M. W. Gill, and M. Head-Gordon, Phys. Chem. Chem. Phys. **8**, 3172 (2006).

[61] A. I. Krylov and P. M. W. Gill, WIREs Comput. Mol. Sci. **3**, 317 (2013).

[62] M. Wormit, D. R. Rehn, P. H. Harbach, J. Wenzel, C. M. Krauter, E. Epivandovsky, and A. Dreuw, Mol. Phys. **112**, 774 (2014).

[63] T. H. J. Dunning, J. Chem. Phys. **90**, 1007 (1989).

[64] A. Schäfer, C. Huber, and R. Ahlrichs, J. Chem. Phys. **97**, 2571 (1992).

[65] S. Horn, F. Plasser, T. Müller, F. Libisch, J. Burgdörfer, and H. Lischka, Theor. Chem. Acc. **133**, 1511 (2014).

[66] F. Plasser, TheoDORE 1.0: a package for theoretical density, orbital relaxation, and exciton analysis, http://theodore-qc.sourceforge.net/

[67] F. Plasser, A. Aquino, H. Lischka, and D. Nachtigallova, in *Photoinduced Phenomena in Nucleic Acids*, edited by M. Barbatti, A. C. Borin, and S. Ullrich (Springer, New York, 2014).

[68] F. Plasser, A. J. A. Aquino, and H. Lischka, J. Phys. Chem. A **116**, 11151 (2012).

[69] F. Plasser and H. Lischka, Photochem. Photobiol. Sci. **12**, 1440 (2013).

[70] E. G. Hohenstein and C. D. Sherrill, J. Phys. Chem. A **113**, 878 (2009).

[71] B. K. Mishra and N. Sathyamurthy, J. Phys. Chem. A **109**, 6 (2005).

[72] P. Petelenz and B. Pac, J. Am. Chem. Soc. **135**, 17379 (2013).

[73] Z. L. Cai and J. R. Reimers, J. Phys. Chem. A **104**, 8389 (2000).

[74] J.-L. Brédas, J. Cornil, and A. J. Heeger, Adv. Mater. **8**, 447 (1996).

[75] D. Moses, J. Wang, A. J. Heeger, A. Kirova, and S. Brazovski, Proc. Natl. Acad. Sci. USA **98**, 13496 (2001).

[76] I. H. Campbell, T. W. Hagler, D. L. Smith, and J. P. Ferraris, Phys. Rev. Lett. **76**, 1900 (1996).

[77] S. F. Alvarado, P. F. Seidler, D. G. Lidzey, and D. D. C. Bradley, Phys. Rev. Lett. **81**, 1082 (1998).

[78] M. Chandross, S. Mazumdar, M. Liess, P. A. Lane, Z. V. Vardeny, M. Hamaguchi, and K. Yoshino, Phys. Rev. B **55**, 1486 (1997).

[79] M. Sun, P. Kjellberg, W. J. Beenken, and T. Pullerits, Chem. Phys. **327**, 474 (2006).

[80] F. Plasser, H. Pasalic, M. H. Gerzabek, F. Libisch, R. Reiter, J. Burgdörfer, T. Müller, R. Shepard, and H. Lischka, Ang. Chem., Int. Ed. **52**, 2581 (2013).

[81] A. Knippenberg, J. H. Starcke, M. Wormit, and A. Dreuw, Mol. Phys. **108**, 2801 (2010).

[82] C. M. Marian and N. Gilka, J. Chem. Theor. Comput. **4**, 1501 (2008).

[83] R. Korytár, D. Xenioti, P. Schmitteckert, M. Alouani, and F. Evers, Nat. Commun. **5**, 5000 (2014).

[84] M. E. Casida, in *Recent Advances in Density Functional Methods, Part I*, edited by D. P. Chong (World Scientific, Singapore, 1995), pp. 155–192.